A Review of Flow Control Techniques and Optimisation in S-Shaped Ducts

Michael M Wojewodka[a,*], Craig White[a], Shahrokh Shahpar[b], Konstantinos Kontis[a]

[a] *School of Engineering, University of Glasgow, Glasgow G12 8QQ, UK*
[b] *Rolls-Royce Plc, Derby DE24 8BJ, UK*

Abstract

This paper is a review of significant studies in the complex flow physics in diffusive, s-shaped ducts, focusing on flow control methods employed to counteract the onset of separation, swirl formation, and non-uniformity of pressure at the duct exit plane. Passive, active, and hybrid flow control, along with optimisation techniques used to control the dominant flow features are discussed.

According to the literature, tapered fin vortex generators and submerged vortex generators improve pressure loss and distortion by double digit percentages, and three-dimensional synthetic jets and pulsed micro-jets show greatest promise amongst active flow control devices. Plasma flow control methods have only sparsely been used in s-ducts with one study performing experiments with alternating-current dielectric-barrier-discharge plasma actuators.

*Please address correspondence to Michael M Wojewodka

Email addresses: m.wojewodka.1@research.gla.ac.uk (Michael M Wojewodka), Craig.White.2@glasgow.ac.uk (Craig White), Shahrokh.Shahpar@rolls-royce.com (Shahrokh Shahpar), Kostas.Kontis@glasgow.ac.uk (Konstantinos Kontis)

The importance of flow unsteadiness has been identified in the literature, with peak values as high as one order of magnitude different from the time-averaged properties. Despite this, very few flow control studies have used time-dependent solution methods to quantify the effect of flow control methods on the unsteadiness of the flow.
Keywords: s-duct, flow control, optimisation

1. Introduction

With operational costs, fuel efficiency, and noise levels of modern airplane engines a prime concern, the s-shaped duct, an example of which is shown in Figure 1, has a number of distinct advantages. Due to the curvature in the duct, the incoming air is slowed down much faster than in conventional straight ducts which leads to shorter designs and considerable weight savings [1, 2]. It is estimated that the net weight of an aircraft would decrease by 15% if the length of the fuselage is reduced by one inlet diameter [3]. Moreover, the curved inlet is a line-of-sight blockage to the engine fan/compressor and thus effectively lowers the noise level as well as radar and infrared signatures [1, 3]. Further weight saving potential exists for unmanned aerial vehicles (UAVs) as their total size is often determined by the propulsion system [2]: a shorter propulsion system would directly relate to a smaller UAV.

S-shaped ducts have been used as intakes on a number of commercial and military airplanes (engines) such as the Boeing 727 (P&W JT8D), the Lockheed Tristar L-1011 (RR-RB211), the General Dynamics F-16 (P&W F100), and the McDonell-Douglas F-18 (GE F404) with the engine buried in the

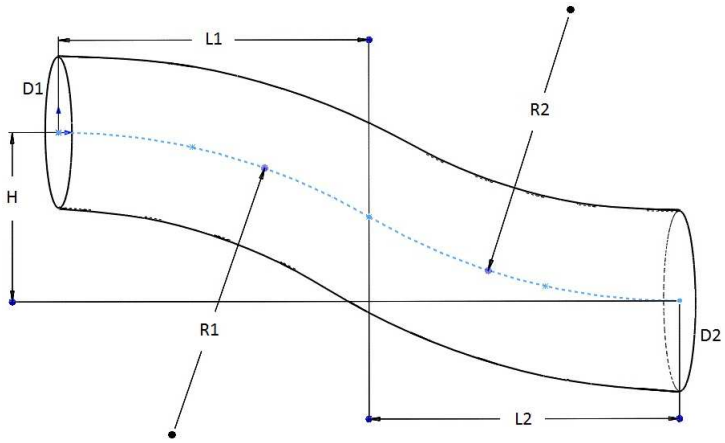

Figure 1: S-shaped duct. Geometry taken from Wellborn [4]. Symbols denote: H = vertical offset; D1 = inlet diameter, D2 = outlet diameter; L1 = horizontal distance to inflection point from inlet; L2 = horizontal distance to outlet from inflection point; R1 = radius of first arc; R2 = radius of second arc.

fuselage. The convoluted s-duct has also been employed to join compressor and turbine stages in turbomachinery. However, the duct design introduces a number of undesirable flow features, such as a non-uniform pressure distribution at the aerodynamic interface plane (AIP), i.e. the plane between the exit of the intake and the compressor/fan of the engine, and flow separation for particularly aggressive convoluted ducts. These undesirable flow features reduce the efficiency of the s-shaped inlets, increase the pressure loss, cause higher levels of fatigue, and hence decrease the operational lives of the engine compressor/fan [3]. Non-uniform flow conditions at the AIP also lower engine surge and stall limits [5].

2. Performance and geometrical parameters

S-shaped ducts are commonly characterised by their diffusion ratio, their radius ratio as well as their length-to-diameter, LDR, and length-to-offset,

LOR, ratios. The diffusion ratio depends on the inlet and outlet diameters denoted by D1 and D2, respectively in Figure 1. The duct's centreline is specified by two arcs with respective radii R1 and R2. The radius ratio is defined by the ratio of the arc radius to the inlet radius.

The two main criteria for evaluating the performance of engine intakes are total pressure recovery and distortion coefficient. The latter one is described by various parameters as is defined in a number of ways [6]. Total pressure recovery (PR) is defined as the mean value of total pressure at the AIP $<P_{\text{t-AIP}}>$ divided by the total pressure of the freestream $P_{\text{t-o}}$ [7], i.e.,

$$PR = \frac{< P_{\text{t-AIP}} >}{P_{\text{t-o}}}. \tag{1}$$

The distortion coefficient used in this review paper is DC_θ. For other definitions the interested reader is referred to [7] and [8]. The distortion coefficient DC_θ is computed by subtracting the minimum mean total pressure of all sectors of extent θ, $< P_{\text{t-}\theta,\text{AIP}} >_{\text{min}}$, (usually equal to 60 degrees) at the AIP from the mean total pressure at the AIP, $<P_{\text{t-AIP}}>$, and dividing the result by the dynamic pressure, q, at the AIP [7],

$$DC_\theta = \frac{< P_{\text{t-AIP}} > - < P_{\text{t-}\theta,\text{AIP}} >_{\text{min}}}{q}. \tag{2}$$

The swirl flow parameter, SC_θ, is based on DC_θ and is defined as the maximum average circumferential component of the cross-flow velocity in a given theta degree sector $MAX<U_{\text{crossflow-}\theta\text{-AIP}}>$ non-dimensionalised by dividing by the velocity on the centreline of the duct at the throat $U_{\text{centreline-throat}}$ [9],

$$SC_\theta = \frac{MAX < U_{\text{crossflow-}\theta\text{-AIP}} >}{U_{\text{centreline-throat}}}. \tag{3}$$

Another swirl flow parameter, the swirl intensity, SI, is defined as the area weighted average of absolute swirl angles for each measurement sector [10]:

$$SI = \frac{\sum_{k=1}^{m} SS_k^+ * \theta_k^+ + \sum_{k=1}^{m} SS_k^- * \theta_k^-}{360}, \tag{4}$$

where θ_k^- and θ_k^+ define the size of the swirl flow regions and SS_k^- and SS_k^+ are symbols for the negative and positive sector swirls, respectively.

Ideally, an s-shaped duct would have small LDR and LOR ratios (i.e. an aggressive design), have a high PR (minimal losses), as well as low DC and SC coefficients for a uniform pressure distribution at the AIP with little swirl flow.

3. Flow physics in s-ducts

First, a schematic drawing (Figure 2) of widely accepted flow features in s-ducts is presented. Figure 2 was created based on findings in the literature.

Depending on the diffusion rate, the radius of curvature and the strength of secondary flows, flow separation is expected near the inflection point [4, 11]. The radius of curvature generates centrifugal pressure gradients that, helped by the diffusion rate, develop into secondary flows and promote a complex three-dimensional flow field [11–13].

The centrifugal body force creates a gradient of pressure between the concave and convex sections of the duct walls [14]. Therefore, the higher velocity fluid is dragged from top to bottom wall in the first bend and from bottom to top wall in the second bend. This accounts for the low velocity region in the upper section of the AIP as slow moving fluid is less affected by the centrifugal pressure gradients.

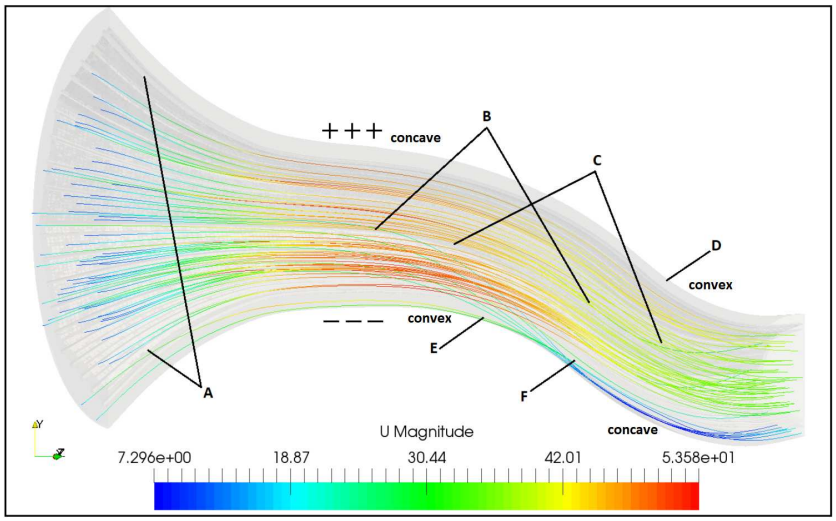

Figure 2: S-duct flow schematic, labelled with the major and widely accepted flow features. On the top side, the +++ indicate a high pressure region and the - - - a low pressure region on the bottom side. Streamlines are coloured with the velocity magnitude in SI units (ms^{-1}). Regions: A) Favourable pressure gradient, thin BL; B) Diffusion causing cross-stream pressure gradients, secondary flow, thickening of BL, and rising static pressure values; C) Radius of curvature promotes centrifugal pressure gradients, cross-stream flow, and swirl formation; D) low energy flow swept to inner wall in second bend; E) Low energy flow swept to inner wall in first bend; F) Separation dependent on diffusion rate, secondary flows, and pressure gradient.

In the curving duct, the static pressure increases at the outer wall, contrary to the inner wall, thickening the boundary layer (BL) [4, 12, 15]. Total pressure losses are most prominent in the lower central region of the AIP and a smaller area at the top of the interface plane [10, 12, 16]. These pressure losses are caused by the secondary flow structures and flow separation in the first bend and the adverse pressure gradient in the second bend, respectively [16].

Contrary to the reported results by Bensod and Bradshaw [17], it is generally agreed that the time-averaged flow is symmetric about the symmetry plane of the s-duct. This was concluded in studies by Taylor et al. [18, 19]

for low to medium Reynolds numbers (Re = 790 and Re = 48000) as well as Vakili et al. [20] and Wellborn [4] for higher Reynolds numbers (Re = $3.25\text{x}10^6$ and Re = $2.6\text{x}10^6$, respectively). This finding has been used extensively in numerical simulations and analysis of the through-flow with only half of the geometry being modelled. In steady, time-averaged, computations this results in a realistic representation of the flow. However, unsteady flow phenomena are asymmetric by nature and hence, this assumption is void for detailed, time-varying simulations of the flow field as demonstrated by Berens et al. [21].

This symmetric flow pattern is dominated by a pair of counter-rotating vortices that form in the duct and propagate to the AIP. Guo and Seddon [22] report a double vortex pattern forming after the second bend. As does Wellborn, stating that a large pair of counter-rotating vortices evolves due to secondary flows dragging fluid from the BL into the core and thus degrading the uniformity of the pressure profile [4]. Swirling flow also develops because the flow along the centreline in a duct moves fastest and hence is subjected to a larger centrifugal force compared to the flow along the duct walls [23]. Blockage, due to flow separation at the duct's inflection point, is responsible for the accelerated core flow [11].

Separation at the inflection point, an example of which is shown in Figure 3, is aided by the adverse pressure gradient, diffusion, and secondary flows. Diffusion causes stream-wise pressure gradients [24], resulting in a non-uniform pressure distribution that promotes separation. The low energy flow in the separated region is affected more than any other part of the flow by the centrifugal pressure gradient associated with the bend, it is hence swept

across the duct to the inner wall as is reported by Guo and Seddon [22]. Brear et al. note that separation creates large unsteady structures, with two vortices being the most distinctive features [25], leading to a reduction in pressure recovery and a high level of unsteadiness. The exact mechanism, cause, and effect of unsteadiness and flow phenomena such as separation, diffusion, and secondary flows is not yet fully understood. However, recent studies have shed some light on the unsteady features of flows in convoluted ducts.

A study by Luers [26] suggests that the distortion coefficient, in this case DC_{60}, does not change with the inlet Mach number. Zachos et al., look at swirl, investigating the flow through an s-duct at Mach numbers in the range 0.27-0.6 [10]. This study concludes that the Mach number has little effect on the flow parameters. Both swirl desccriptors, SI and SC_{60}, increase very weakly with higher Mach numbers as is shown in Figures 4 and 5.

Unsteady flow measurements were conducted by Gil-Prieto et al. in two circular s-shaped ducts at Mach numbers of 0.27 and 0.6 [13]. They compared two ducts with two height-to-length ratios H/L, of 0.5 and 0.27, respectively. It has to be noted that the snapshots of the flow were underresolved temporally and the unsteadiness was quantified by a sample of statistically representative data. Results show that the instantaneous flow features are different from the time-averaged properties. The difference in peak values of swirl distortion, for example, can be one order of magnitude higher. Figure 6 shows the time averaged field and the standard deviation of the pressure recovery and swirl at the AIP. The results are based on numerical analysis of Delayed Detached Eddy Simulation (DDES) and are adapted from [27].

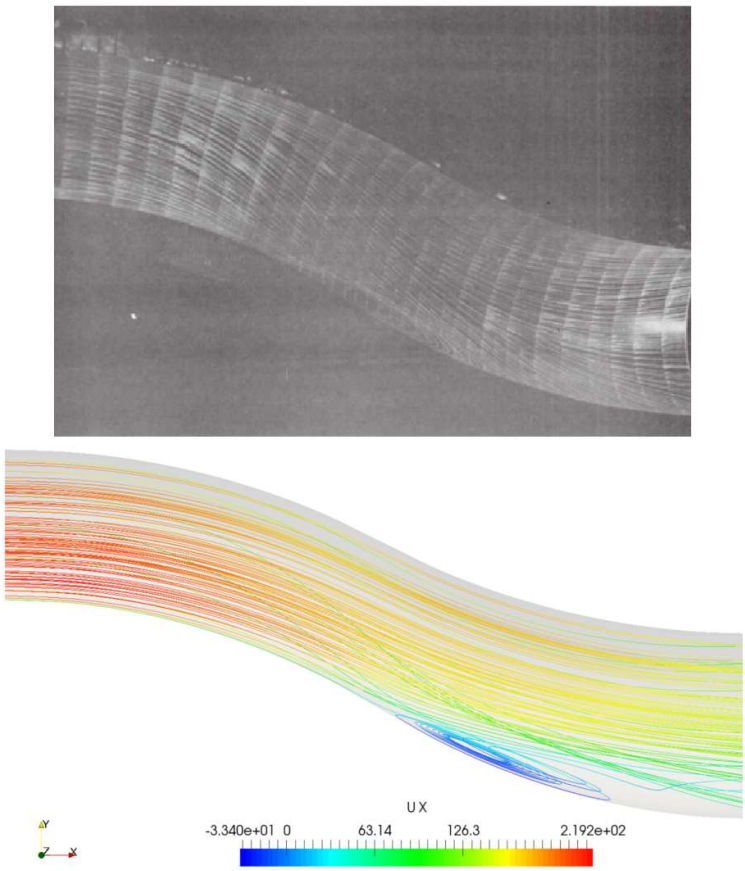

Figure 3: Flow separation in convoluted duct at a Mach number of 0.6. Top: Wellborn's experimental oil-flow results [4]. Bottom: Authors' CFD simulation with OpenFOAM. Streamlines are coloured with the streamwise velocity in SI units (ms^{-1}).

This finding could lead to design changes downstream, i.e. in fan geometry, or the integration of complex intakes.

Based on the analysis of stereoscopic PIV data, dominant modes of flow structures are identified in a follow-up study by Gil-Prieto et al. [28]. The results clearly show a switching as well as a vertical mode. In the switching mode, the vortices observed in the mean flow alternate in strength with either one dominating the flow pattern at the AIP - perturbing the circumferential

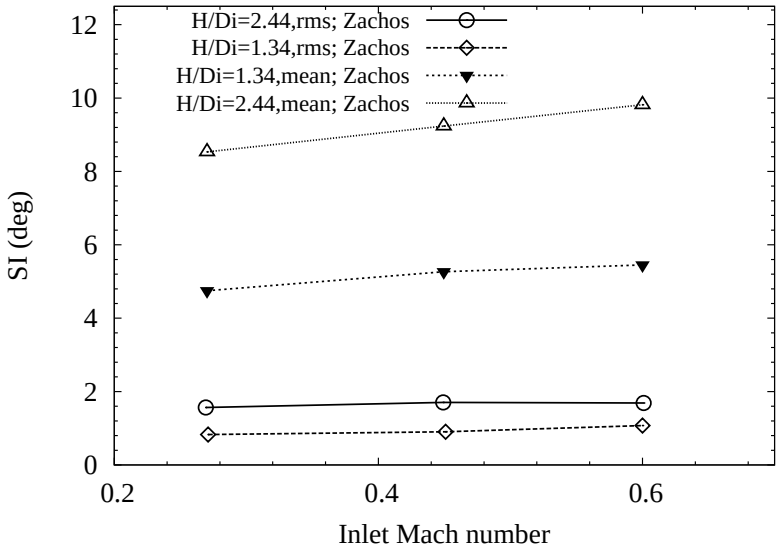

Figure 4: Swirl intensity vs inlet Mach number. Data replotted from [10].

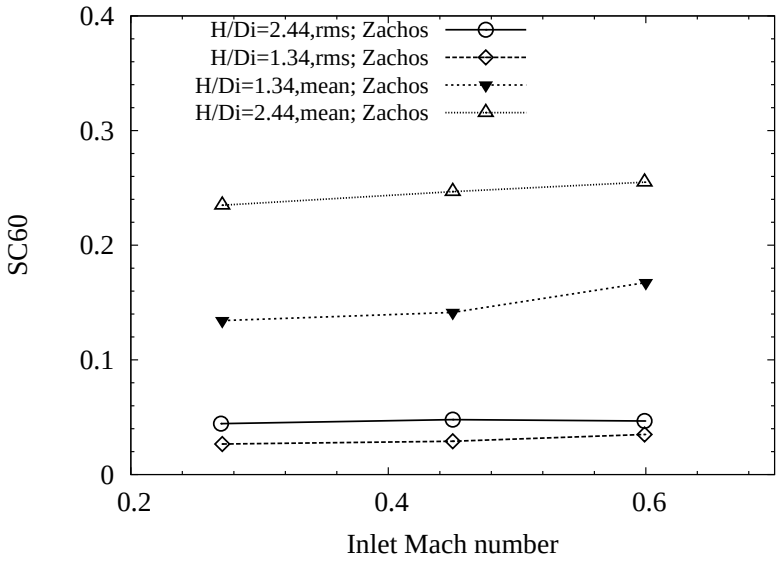

Figure 5: Swirl coefficient SC60 at AIP vs inlet Mach number. Data replotted from [10].

flow field. Gil-Prieto et al. postulate that the vertical mode is associated with unsteadiness of the centreline shear layer. Its effect is to shift the vortical

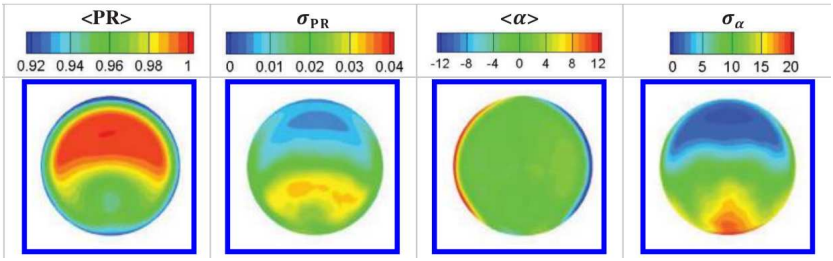

Figure 6: Average and standard deviation of pressure recovery and swirl at AIP of Wellborn duct based on DDES simulation. Figure adapted from [27].

structures, and hence the main loss region, vertically from its time-averaged position (see Figure 7).

The described flow features are undesirable and much research has focussed on ways to improve the flow at the AIP, using flow control devices, or geometry optimisation.

4. Passive flow control

4.1. Working principle of common passive flow control devices

Spoilers are commonly used as a swirl control device. The spoiler trips the flow which causes separation and a decrease of the total pressure. A reduction in pressure gradients has a direct effect on swirl formation. Fences and rails are also used to the same effect.

Vortex generators (VG) are mainly used to control separation. They re-energise the low momentum fluid in the boundary layer by generating vortical structures that draw higher momentum fluid from the core flow in to the boundary layer. This mechanism delays the onset or prevents separation of the BL. Vortex generators also introduce a secondary flow pattern within the BL that, ideally, counters the naturally occuring one and prevents the formation of the pair of counter rotating vortices [29]. Vortex generators come

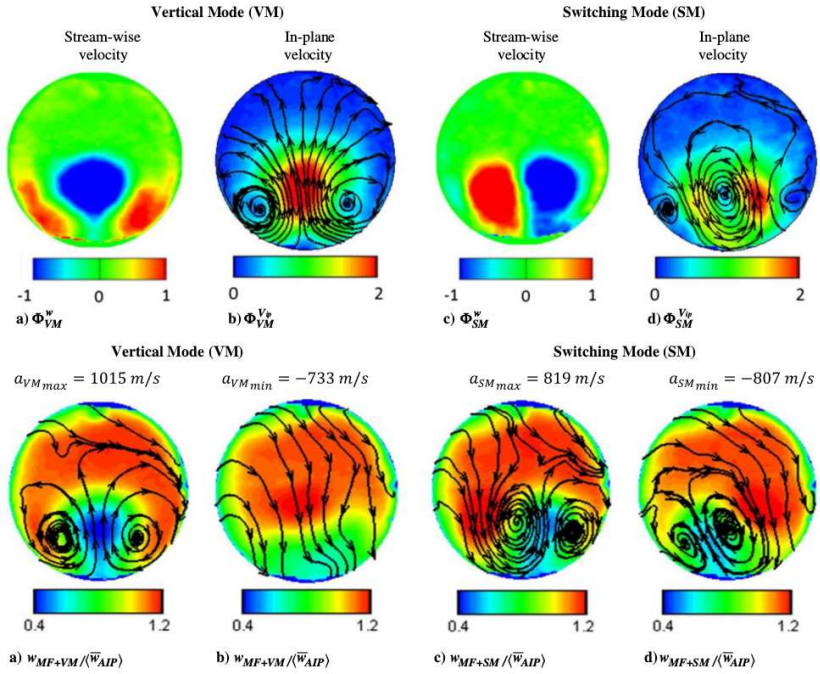

Figure 7: Switching and vertical modes (SM and VM respectively) at Mach number of 0.27. Figure taken from [28]. Top: Proper orthogonal decomposition (POD) modal shapes with a) symmetric distribution for the streamwise velocity component of the VM; b) vertical in-plane perturbation (VM); c) anti-symmetric distribution of the switching mode; d) swirling perturbation of the in-plane velocity. Bottom: Snapshots of vertical and switching modes superimposed on the mean flow in the duct with a) showing the effect of the VM on the mean flow with a positive temporal coefficient, and b) with a negative temporal coefficient. The superimposed SM on the mean flow is shown in c) and d) for a positive and negative temporal coefficient, respectively.

in different shapes and sizes. Schematic diagrams of vane type, tapered-fin, and wishbone vortex generators are shown in Figure 8.

Submerged VGs have a much lower device drag than conventional VGs [30] - Lin [29] reports a difference of an order of magnitude. Conventional VGs can produce too strong vortices, due to their relative height compared to the boundary layer thickness (δ), that do not attenuate and disturb the flow past their intended range. However, in s-ducts a high rate of vortex decay

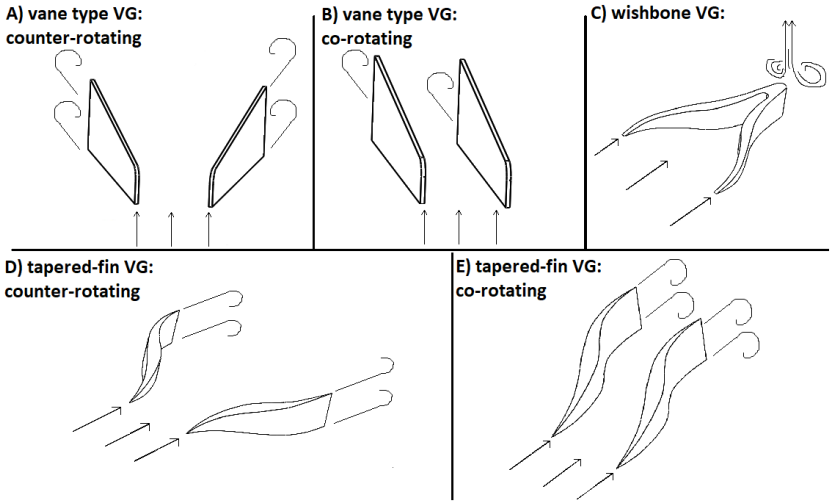

Figure 8: Schematic representation of various VG types: Counter and co-rotating configurations of vane type VG in a) and b) respectively. Wishbone VG in c). Counter and co-rotating configurations of tapered-fin VG in d) and e) respectively.

is desirable once short-range flow control is achieved. The effectiveness of submerged VGs is in part attributed to the turbulent BL they are placed in. As the turbulent BL has a fuller velocity profile than a laminar one, the submerged VGs have a higher velocity to work with and hence create stronger vortices than in a laminar BL of similar height. The local velocity at 20% height in a typical turbulent BL is already 75% of the freestream value [31].

Detrimentally, vortex generators, spoilers, fences, and rail devices cause an obstruction to the flow, and have an associated drag penalty. From these four devices only the VG are positioned axially, i.e. in the streamwise direction, so that the drag penalty is the smallest as they cause the smallest obstruction to the flow.

4.2. Passive flow control devices employed in s-shaped ducts

Spoilers can be used to alter the swirl pattern and create a zero swirl flow as demonstrated in a rectangular-to-circular cross-section s-duct by Guo and Seddon at 40 ms^{-1}. A solid spoiler of 0.13w (where w is the ratio of spoiler width to duct width at throat) gives a zero swirl coefficient [9]. However, its side-area results in high drag at low incidence flows, and hence high pressure losses. In a similar study, swirl reduction by using spoilers was also demonstrated in convolued ducts (U=38 ms^{-1}, Re = 3.8x10^5), with both horizontal and vertical offsets [32]. Vakili et al. used a thick rail device of thickness equal to the BL height, to successfully control swirl formation and eliminate flow separation [20] in an s-duct of circular cross-section (Ma = 0.6, Re = 3.25x10^6). As in Guo and Seddon's study [9], this also resulted in losses due to a high induced drag and blockage to the flow. The distortion coefficient, DC_{60}, at the AIP was degraded (from 0.559 to 0.772) by the rail device.

Reichert and Wendt [33] used arrays of wishbone VG in the Wellborn s-duct. The study looked at VG streamwise location, their spacing, and their height (40%, 100%, and 160% of BL height). Even though some configurations were effective in improving pressure recovery, no configuration tested managed to reduce pressure distortion values at the AIP. This may be partly due to the counter-rotating vortices produced by each wishbone VG. Counter-rotating vortices interfere with one another resulting in vortex interference and a reduction in vortex strength [34]. Marginal effects on the flow of wishbone VG of height equal to 60% of the BL thickness have also been reported by Sullerey [24] as they are best suited for flows with non-zero sideslip

angle which is not the case in s-ducts upstream of the separation point. Lin, also, concludes that co-rotating configurations tend to yield better results in s-ducts [29].

Vane type vortex generators were used by a number of researchers [20, 35–39]. Two publications embedded counter-rotating configurations and report beneficial effects on the flow such as a supressed separation region and reduced total pressure losses [37] or a more uniform flow at the AIP [20]. However, the former study was conducted on a constant-area cross-section s-duct which does not take into account the added complexity of the flow due to diffusion. The latter does not provide essential information on the location of the actuators, their number, and their height with respect to the BL thickness.

Five co-rotating VG configurations were tested by Delot et al.[36] with varying angle to the incoming flow and of various heights (6, 4, and 2 mm - BL thickness information is not provided). The greatest reduction in DC_{60} is achieved with the highest VG and a constant orientation to the incoming flow of 18 degrees. Zhang et al. compared counter and co-rotating vane type VG in the same convoluted duct at a Reynolds number of $1.5x10^5$[38] with heights of 25% and 15% of the BL thickness, respectively. Other geometric parameters and their number (2 pairs in the counter-rotating set-up and 4 single VG in the co-rotating set-up) were identical for both configurations. Zhang and collegues report that both configurations were successful in eliminating separation (based on oil flow visualisations and surface pressures) and resulted in an identical distribution of static pressure. This is also evident from oil flow visualisations presented in Figure 9. However, the counter-

rotating VG array produced higher near-wall losses and a less uniform flow at the AIP. The co-rotating array decreased the pressure loss at the AIP by 5%, 1% more than the counter-rotating configuration.

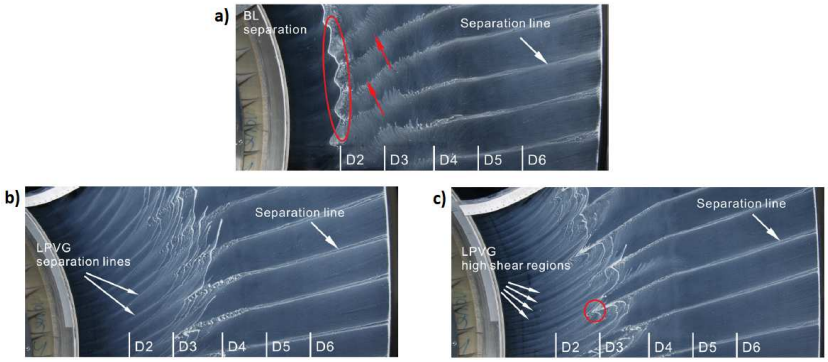

Figure 9: Oil flow visualisation of baseline (a), co and counter-rotating vane VG (b) and (c), respectively. In a) flow separation is clearly visible (marked with red oval). This separation region is eliminated by the co and counter-rotating VG configurations in (b) and (c), respectively. Figure taken from [38].

Paul et al. [14, 40] have managed to use counter-rotating vane type VG, called fishtail VG in the publication, in s-ducts and improve performance parameters - flow uniformity improved at the AIP (16% lower distortion [14]), higher static pressure recovery and reduced total pressure loss [40]. Submerged VG of height of 0.2 δ were placed at the inlet at both the bottom and top surfaces of the convoluted duct. With the height of the VG being a fraction of the BL thickness, counter-rotating VG gain effectiveness as their vortices remain within the BL re-energising the low-momentum fluid but do not disturb the flow past their short-range flow control objective. Combining submerged VG with a chamfered inlet area (23% at inlet and 12% at exit is blocked with a fillet) Paul et al. show that flow uniformity is improved significantly [14] as is the pressure loss coefficient (Figure 10). This might be

due to the fact that the rectangular cross-section is made more circular by the fillets which reduces corner losses through the s-duct.

Reichert and Wendt employed arrays of tapered fin VG of height equal to the BL thickness in the Wellborn s-duct at a Mach number of 0.6 [5]. The study investigated narrow and wide spacings between consecutive VG. Based on the results, configurations of narrow spaced VG shed vortices that did overcome the natural secondary flows and are better equipped to improve pressure recovery and eliminate separartion. This is believed to be the case as vortices of narrow configurations experience interference effects and merge into a single pair of vortices. Wide spaced arrays, however, retain their separate vortices and have an effect on a wider circumferential extent hence, the uniformity was highest with wide spaced configurations. Wendt et al. explain in their study on structure and development of streamwise vortex arrays that the downstream interaction depends on the VG spacing. Tight arrays provide best local mixing hence are better equipped to supress flow separation, but their vortices attenuate rapidly downstream [35].

Tanguy employed vane type VG in an experiment with unsteady measurements to control the flow through an s-duct [16]. This study (Ma = 0.27 & 0.6), which is temporally underresolved and bases its conclusions on statistics of flow snapshots, examines the effect of the circumferential extent, the VG height, and the axial location. All configurations were successful in improving the pressure recovery and decreasing pressure losses, but four designs increased the distortion levels at the AIP [16]. It was found that the smallest VG height (equal to 0.63 of BL thickness), and an axial placement of 14 δ upstream from the separation point (i.e. configuration VG5 in the

publication), resulted in the best performance improvement.

The effect on swirl at the AIP is also quantified in the study by swirl descriptors [16]. The study shows that dynamic levels of swirl angle can be significantly reduced. Tanguy et al. explain the beneficial effect with the increased secondary flow field which confines the swirling flow to their respective regions, reducing unsteadiness across the AIP. For example, one of the VG configurations decreased the mean swirl intensity, SI, by 49% with a significantly lower standard deviation and maximum SI values.

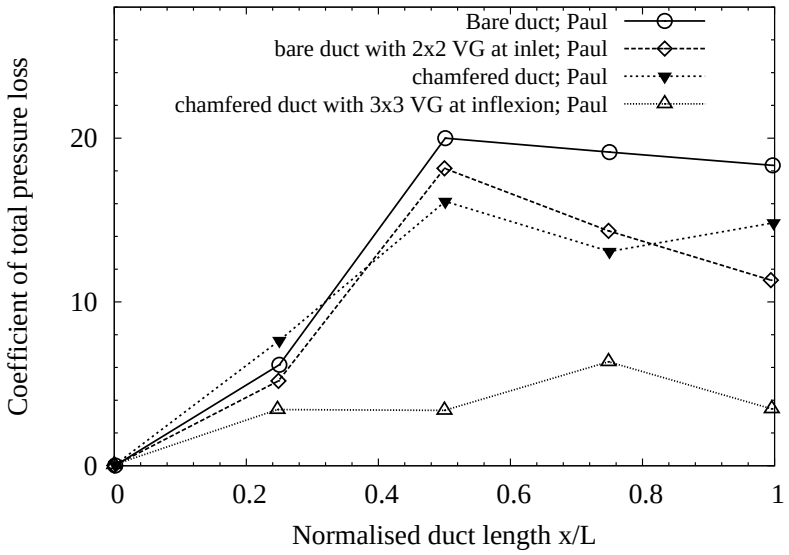

Figure 10: Coefficient of total pressure loss along the duct length. Data replotted from [14].

Conventional VGs are usually placed further downstream than submerged VGs, 5δ and 2δ upstream of the baseline separation location, respectively [29]. Jenkins et al. [41] report that the location of submerged VG should be 5-30 device heights upstream of the separation location. It is widely agreed that the optimum location for vortex generators is upstream of the separation

point just ahead of the high adverse pressure gradient [24, 37]. At this location the boundary layer grows rapidly before detaching from the surface and separating. Sub VGs lose effectiveness for heights smaller than 0.1δ. The smaller its height, the stronger the influence of the wall and the shear stress on the produced vortices. This promotes faster vortex strength decay and hence less flow control authority. Joint vane type VG, or VG in close proximity to one another producing counter-rotating vortices, experience interference effects and a reduction in vortex strength [34]. Therefore, co-rotating configurations tend to work better in s-duct geometries [29].

Table 1 is a summary of all the passive flow control techniques considered in this review paper. The summary indicates which techniques were found to improve or deteriorate flow phenomena such as separation, distortion at AIP, swirl flow, pressure loss, and pressure recovery. The table also shows the flow regime, characterised by the Reynolds number or Mach number of the flow, as well as the publication the results were reported in. The column labelled "study" indicates through the letters "E" and "N" whether a study was performed experimentally, numerically or both.

Different geometries and flow regimes for the studies presented in Table 1 prevent the results from being directly comparable to each other, but, a comprehensive overview is obtained. Reducing the extent of separation usually has a positive effect on pressure loss and pressure recovery, however, this is not assumed in the summary so that only explicitly stated results from the corresponding publications are included.

Table 1: Summary of passive flow control techniques employed on s-ducts

flow control	flow regime	separation	distortion	PR	pressure loss	swirl	E/N	publication
spoilers	Re=4.2x10^5	↓	/	↓	↓	↑	E	[9]
rail	Re=3.25x10^6	↑	↓ 38%	↓ 13%	/	↓	E	[20]
wing type VG	Re=3.25x10^6	↑	↑ 18%	↑ 9.9%	/	↑	E	[20]
vane type VG (const. area)	Re=4.73x10^4	↑	/	/	↑	↓	E	[37]
tapered fin VG	Re=2.6x10^6	↑	↑ 50%	↑ 0.65%	/	↑	E	[5]
tapered fin VG (duct1)	Re=0.78x10^6	/	↑ 9%	↑ 8.4%	↑ 11%	/	E	[24]
tapered fin VG (duct2)	Re=0.78x10^6	/	↑ 17%	↑ 20%	↑ 38.8%	/	E	[24]
wishbone VG (duct2)	Re=0.78x10^6	/	↑ 5%	↑ 0.7%	↑ 13.5%	/	E	[24]
fences (duct2)	Re=0.78x10^6	/	↑ 10%	↑ 12%	↑ 28.8%	/	E	[24]
fences (duct1)	Re=0.78x10^6	/	↑ 11%	↑ 18.6%	↑ 37.5%	/	E	[24]
VG	Re=2.6x10^6, Ma=0.6	↑	↑	↑	↑	/	E	[33]
VG vanes	Re=1.5x10^6	↑	↑ 50%	↑	↑	/	E	[36]
subm. VG + chamfered corners	Re=1.34x10^5	/	↑ 16%	↑	↑	/	E	[14]
subm. vane type VG	Re=0.68x10^5	↑	↑ 27%	↑ 27%	↑ 14%	/	E&N	[40]
VG	Ma=0.27	/	- - -	↑	↑ 25%	↑	E	[16]
VG	Ma=0.6	/	- - -	↑	↑ 30%	↑	E	[16]
BL fences	Ma=0.85	/	↑ 11%	/	↓ 52%	/	E&N	[42]

Symbols indicate: ↑ = improvement by flow control technique; / = not reported; ↓ = deterioration by flow control technique;
- - - = no effect.

4.3. Optimisation studies

Optimisation techniques were used by a number of researchers to alter flow control actuators [43–46] or the geometry [47–50] of convoluted ducts and thus mitigate undesirable flow features. Optimisation algorithms can be broadly split into three groups: evolutionary based algorithms, local search methods, and mid-range approximation methods.

Evolutionary based optimisation methods are based on natural selection principles of evolution and mutation [51]. Different designs are rated according to their goodness criteria, i.e. depending on the value of their corresponding cost function. The higher a particular design is rated the greater its chance to 'reproduce' and influence the next generation of designs. These algorithms are generally able to find a global optima, however, a considerable number of design evaluations are required to reach a final answer. An example of evolutionary optimisation algorithms is the adaptive range multi-objective genetic algorithm, ARMOGA [52].

Local search methods make use of adjoint gradients which are used to compute the sensitivity of a baseline design with respect to local changes. As pointed out by Shahpar et al. [53], the sensitivity of a parameter can be divided into parts relating to changes in the flow and of the geometry. For the adjoint method to work, an existing, well-converged computational fluid dynamics (CFD) solution is required, as the gradients are computed on this basis.

Mid-point approximation methods (MAM) are based on the trust region approach in which the optimiser searches for an optimum solution. The trust regions are gradually reduced in size during the optimisation process

as the design space is narrowed down. Approximate models are built on each trust region with a response surface model (RSM) forming the basis for the next design evaluations [54]. An advantage of using the combination of approximate models is that this method is considerably faster (between 6 to 10 times) than genetic algorithms [55]. Examples of such algorithms are multi-point approximation methods [56, 57] (MAM1 and MAM2) that are being developed.

Sequential quadratic programming (SQP) algorithms are iterative optimisers for non-linear problems. The algorithm solves a number of sub-problems optimising a quadratic model [58]. The solution approximations are used to create a more appropriate solution in the next step. Convergence is achieved by iterating through the process until a solution cannot be improved upon further. As the solution is based on the initial approximation to the algorithm, SQP works best with a good initial guess, but does not handle noisy data well.

Usually, the numerical cost of an optimisation study increases with increasing number of design parameters (d.p.), as a bigger design space has to be searched and evaluated by the algorithm.

4.3.1. VG optimisation

Geometrical features of VG and their location (5 d.p.) in a circular s-duct (Ma = 0.66) were optimised using a RSM search based on 27 CFD runs by Jirasek [44]. The RSM search indicated that the most important parameters with respect to minimising the pressure distortion are the VG height and their distance from the separation region. With respect to increasing the pressure recovery, the angle of inclination and square of the VG height are the

most important terms. Performance parameters were improved significantly based on the optimisation study with distortion reduced to 7% from 56% and pressure recovery increased by 0.66%. An earlier study by Hamstra et al. [43] utilised a design of experiment (DoE) approach based on 45 CFD Reynolds Averaged Navier-Stokes (RANS) simulations for micro-jet and micro-vane VG (6 d.p.) at an inlet Mach number of 0.6, improving both the distortion and pressure recovery in the duct.

Anderson et al. [45] also employed the DoE - RSM combination to investigate micro-vane and micro-jet actuators at a Mach number of 0.7. Their optimisation strategy allowed for identifying two-factor synergistic effects of the three variables used: number of micro-vane actuators (n), their height (h), and cord length (c). The results suggest that there is a coupling effect between the number of actuators and their height (n & h), as well as their cord length (n & c), that is important for controlling the inlet total pressure recovery. Three two-factor interactions (n & h, n & c, and h & c) were found to influence the DC_{60} coefficient at the AIP.

Another study optimising VGs by Yi et al. [46] used an adjoint code to optimise an array of 11 VGs resulting in 55 d.p. in total (5 d.p. per VG: chord length, height, angle of incidence, axial position, circumferential position) in an s-duct of circular cross-section. The objective was to minimise the distortion coefficient, with the baseline total pressure recovery defined as a constraint (lower limit) to ensure pressure loss would not be increased. The optimised configuration improved distortion by 79% and also yielded improvements at a number of off-design conditions. Total pressure recovery also improved as is evident from the contours presented in Figure 11.

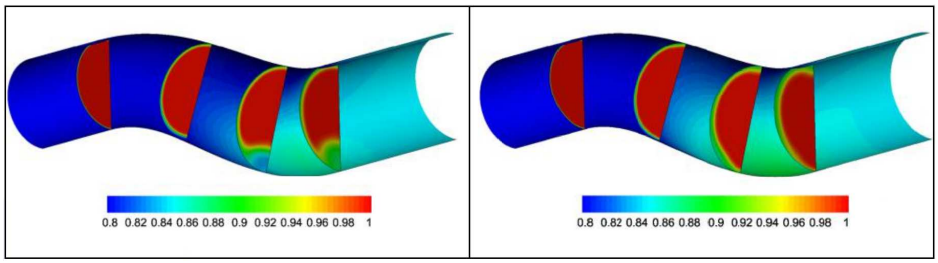

Figure 11: Normalised total pressure recovery contours for convoluted duct without (left) and with (right) vortex generator array. Figure taken from [46].

4.3.2. Geometry optimisation

Zhang et al. [47] conducted an optimisation study using an SQP algorithm with two design parameters and distortion at the AIP as the objective function. The two design parameters were controlling the height and width of a perturbation introduced just ahead of the onset of flow separation. The perturbation in the duct geometry introduces a separated flow region, reducing the cross-flow, and resulting in a reduction of distortion of 63% at the AIP. The pressure recovery remained unchanged as the separation in the bump behaved like a closed bubble and was confined to that region [47].

In a similar study, the Wellborn s-duct was used for an optimisation study of a bump with two design parameters (height and stream-wise width of bump) and one objective function (minimising distortion), using a gradient based feasible SQP optimiser [48]. Reducing the distortion by 37%, the optimised design has an increased bump ahead of the separation region similar to the one presented in reference [47]. This leads to an area increase and a reduction of secondary flow as reported by Lefantzi and Knight [48]. This is consistent with other optimisation studies that base the performance criteria on RANS simulations.

However, as noted previously, RANS simulations are not suitable to capture the full dynamics of the complex flow field in diffusing, s-shaped ducts. By inspection of the optimised duct geometries in [47] and [48], it is highly likely that the benefits would be outweighted by the expected unsteady distortion such designs would naturally promote. Moreover, unless embedded in the fuselage, the external aerodynamics over such geometries would be highly susceptible to separation and increased drag, making such design solutions not acceptable from an applications perspective.

Geometry optimisation based on a multi-objective genetic algorithm (MOGA) was used by Aranake et al. on an s-duct (Ma = 0.3) including two design objectives: maximisation of total pressure recovery and minimisation of distortion [49]. The optimisation was only partly successful, as the total pressure recovery of the optimised designs was of the same order of magnitude as for the baseline case. However, the distortion coefficient was significantly reduced by 56% and 50%, according to numerical and experimental data, respectively. The lowest distortion was achieved for the largest area ratio at mid span leading to the following design suggestion: "The flow in the approximate midpoint of the bends should be over-expanded, i.e. the cross-sectional area should be greater than the outlet cross-sectional area." [49]. Due to the over-expansion, the BL separates earlier generating more mixing of the flow, which, together with the favorable pressure gradient resulting from the contraction, leads to a smaller distortion coefficient at the duct outlet [49].

A combined low and high fidelity optimisation was conducted by Ghate et al. [50]. The low fidelity study used a SQP algorithm optimising pressure

recovery, while the high fidelity optimisation minimised distortion through a DoE and RSM search. The low fidelity optimisation produced designs with area expansion over the first one third of the duct's length, with constant area thereafter and a 1.5% increase in pressure recovery. The high fidelity optimisation reduced the distortion coefficient from 6.19 to 1.7, with a much more uniform pressure distribution at the exit plane.

It is important to note that all of the research studies presented in this section are based on steady-state RANS simulations. While it has been established that the time-dependant flow field properties are important in convoluted ducts, unsteady simulations still seem to be too computationally expensive to be employed in optimisation studies due to the high number of CFD runs required. However, with computational resources becoming more readily available, optimisation studies should not only include the uniformity of the flow at the AIP but also the unsteadiness. As a compromise, to minimise the computational expense of the simulations, at least the optimised geometries should be analysed with unsteady CFD.

Table 2 gives a summary of all optimisation studies reported in this section in a similar fashion to Table 1.

5. Active flow control

One of the earliest studies to employ active flow control in s-ducts was conducted by Ball in 1985 [59], using wall suction and blowing at a Mach number of 0.7. Pressure measurements suggest that separation was eliminated and effective boundary layer control achieved, using a slot blowing a mass flow equal to 2% of the inlet flow. Automatic adjustable blades (AABs) were used as a swirl control mechanism by Weng and Guo in 1991 [60]. This

Table 2: Summary of optimisation techniques employed on s-ducts

flow control	flow regime	separation	distortion	PR	pressure loss	swirl	E/N	publication
microvane VG	Ma=0.6	↑	↑ 50%	↑ 5%	↑	/	E&N	[43]
microjet VG	Ma=0.6	↑	↑ 20%	↑ 2.5%	↑	/	E&N	[43]
VG and location	Ma=0.6	/	↑ 87.5%	↑ 0.66%	/	/	N	[44]
VG	Ma=0.27	/	↑ 79%	- - -	/	/	N	[46]
bump in geometry	Re=2.6x10^6, Ma=0.6	/	↑ 63%	- - -	/	↑	N	[47]
geometry	Ma=0.3	/	↑ 56%	- - -	/	/	E&N	[49]
cross-sectional area	Ma=0.52	/	↑ 72.5%	↑ 1.5%	/	/	N	[50]
bump in geometry	Re=2.6x10^6, Ma=0.6	/	↑ 37%	- - -	/	↑	N	[48]

Symbols indicate: ↑ = improvement by flow control technique; / = not reported; ↓ = deterioration by flow control technique;
- - - = no effect.

method reduced the bulk swirl to the point of elimination at 7.5 degree AAB angle in a rectangular-to-square cross-section s-duct, without changing the pressure distribution along the walls. However, AABs also resulted in a slightly higher pressure loss in the core flow [60].

Synthetic jets (blowing velocity = 11 ms^{-1}, frequency = 1032 Hz) were employed in an s-duct by Amitay, with results suggesting complete flow reattachment and higher pressure at the AIP for Ma<0.2 and faster flow reattachment for 0.2<Ma<0.3 [61]. In another study, synthetic jets were also found to suppress flow separation and decrease pressure distortion in an s-duct at a Mach number of 0.43 [3]. Figure 12 shows the three actuation cases tested. The results show that 3D actuation in the middle of the duct, i.e. Figure 12c, is more effective than the 3D actuation along the sides of the duct (Figure 12d), or the 2D actuation (Figure 12b) along the whole span. The cross-flow velocity presented in Figure 13 is lowest for the 3D actuation case with synthetic jets applied in the middle of the duct closely followed by the 2D actuation. It is worth pointing out that the 3D actuation along the sides of the duct (Figure 12d) does not reduce the cross-flow velocities which stay at the same level as for the bare duct.

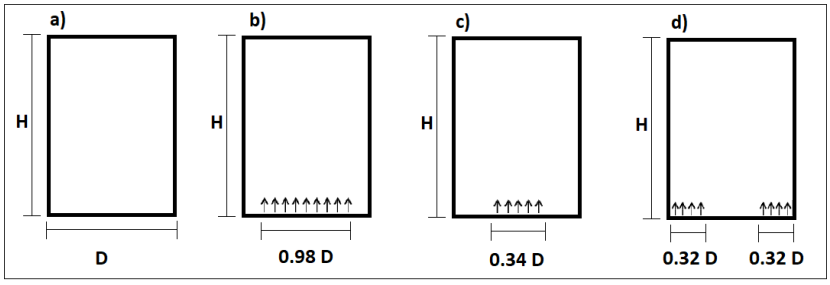

Figure 12: Sketch of synthetic jet actuation positions: (a) no control, (b) up, (c) up-mid, and (d) up-side [3].

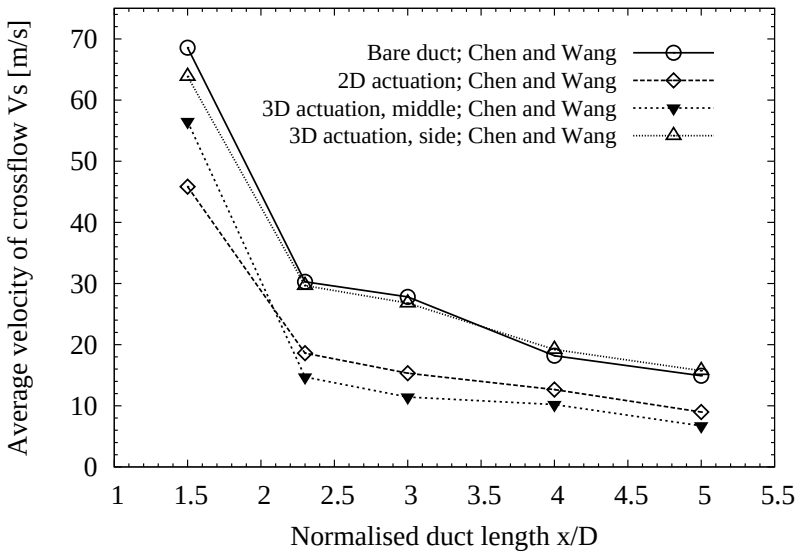

Figure 13: Average secondary (cross-flow) velocity [ms^{-1}] vs nondimensionalised duct length for control cases a, b, c, and d as in Figure 12. Data replotted from [3].

Luers [26] investigated wall jet injection (as a percentage of inlet mass flow) at the separation point and upstream of this, in an s-duct (Ma = 0.5-0.7), for different inlet mass flow conditions. Pulsed actuation proved to be the most effective with a frequency equal to the shedding frequency of vortices in the undisturbed flow. Increased values of pressure recovery and lower distortion were measured [26]. Figures 14 and 15 show the pressure recovery, and improvement in pressure recovery, for a number of jet injection mass flows and two inlet mass flow conditions, respectively. It is clear that the beneficial effect of the wall jet on the pressure recovery increases initially with percentage injection mass flow, but saturates for 3-4% of the inlet mass flow.

VG jets in circular and rectangular-to-circular cross-section s-ducts (Ma = 0.1, Re = 7.8x10^5) were used with a fixed pitch angle of 45 degrees and

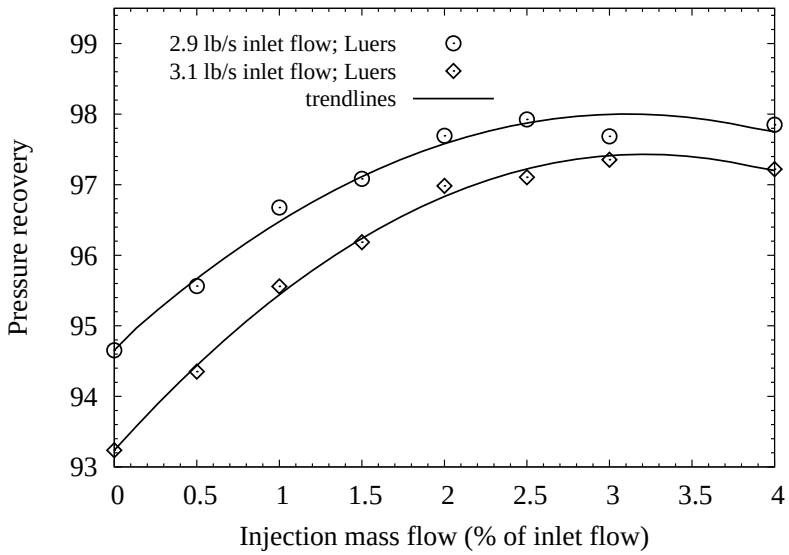

Figure 14: Pressure recovery at AIP vs injection mass flow as % of inlet flow. Data replotted from [26].

a range of skew angle [62]. A skew angle of 135 degrees resulted in the best performance. Jet-to-freestream-velocity ratios of 1.6 and 1.7 in the two circular and rectangular-to-circular ducts respectively give the best pressure recovery values. For the circular s-duct, Pradeep and Sullerey record a 20% reduction in total pressure loss and a 30% reduction of turbulence intensities at the AIP [62]. Tangential blowing (14 tubes, blowing velocity 12.5 to 24.5 ms^{-1}) and VG jets with the same momentum coefficient as the tangential blowing, were investigated by Ng et al. [37] in a constant area s-duct (R = 4.73x10^4) and were placed on the near-side wall. They suppressed flow separation successfully, but also lead to an increased swirl in the flow at the AIP. As stated by Vaccaro et al. [63], a 2D control jet actuator in an s-duct (Ma = 0.43) can affect centreline reattachment, but cannot influence the formation of secondary flows, and does not reduce pressure losses at off-centreline lo-

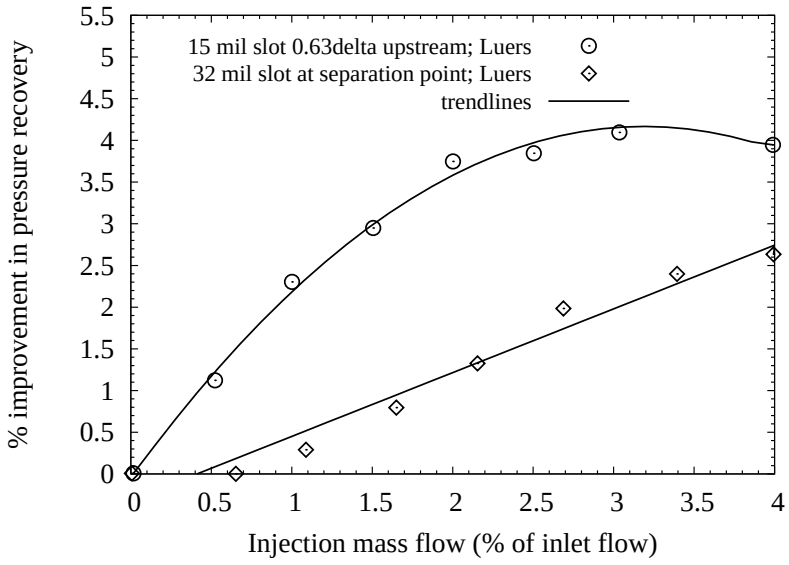

Figure 15: Improvement of pressure recovery at AIP in % vs injection mass flow as % of inlet flow. Data replotted from [26].

cations of the AIP. Vaccaro et al. suspect that the two-dimensional jet does not influence the three-dimensional flow features enough to have a significant effect on the performance parameters of the flow.

Another study by the same researcher, using 2D steady blowing through a continuous slit spanning 90% of the duct along the lower surface of an s-duct with a similar Mach number (Re = 0.75x10^6, Ma = 0.44), managed to reattach the flow along the centreline, decreasing the flow speed and improving the flow at the AIP. Pressure recovery increased by 1.7%, there was a 13.3% reduction of standard deviation in the pressure signal, and elimination of the dominant frequency of St of 0.26 [2]. The study also shows that unsteady forcing, at frequencies of St of 0.26, 0.59, and 0.88, did not have the same beneficial effect as steady actuation. Supersonic pulsed jets (7 jets per half configuration) in an s-duct (Re = 1.5x10^6) resulted in fully reattached flow

in a study by Garnier et al. [64], with jets of Ma 1.4 out-performing jets with Ma 2. Garnier et al. recommend the use of higher pulsed actuation frequencies than those present in the flow at the separation region.

In a further study, actuation with pulsed jets (14 actuators, 0 to 1000 Hz) in an s-duct (Re_{max} = 1.5x10^6, Ma = 0.2-0.4) show that the efficiency of actuators decreases with increasing Mach number [65]. Nonetheless, a 1% gain in efficiency was achieved for the Mach 0.4 case. A zero-net-mass-flow jet was created with a 4.5mm displacement of the oscillating piston and a frequency of 28.8 Hz. This is a momentum influx device that does not add more mass to the flow. Mathis et al. [66] employed this technique in an s-duct (Re = 4.1x10^4) for a low Reynolds number flow eliminating the separation region completely. However, drawbacks of this technique include added complexity through moving parts and weight addition.

Electrohydrodynamic (EHD) glow discharge plasma (no additional mass flow or moving parts) was used in an s-duct (Ma=0.3 to 0.7) by Hui et al. in a numerical study, resulting in a maximum improvement of 6.7% for pressure distortion and 0.34% for pressure recovery [1]. Another study that demonstrated the suitability of plasma for internal flow control was conducted by Xu [67]. The author successfully used AC-DBD plasma actuation (dielectric barrier discharge plasma powered with an alternating current wave form) in an s-duct to reduce the extent of the separation region. The optimal location for actuators was found to be near the separation point for both continuous and pulsed actuation. As expected, separation reduction increases with increasing actuator strength [67]. AC-DBD plasma, however, is self-limiting, with the highest recorded values of induced flow being of the magnitude of 10

ms^{-1} [68], which is not fast enough to influence the flow structure in s-shaped ducts and prevent separation at high subsonic flow speeds.

A different form of plasma generation, referred to as NS-DBD plasma (dielectric barrier discharge plasma powered with a nano-second pulse wave form) does not exhibit this self-limiting behaviour [69]. No publications of NS-DBD plasma actuation in s-shaped ducts were found during the literature review. However, its applicability to flow control in general has been demonstrated in a number of studies on aerofoils [69–71].

Finally, a study comparing passive to active flow control in the same s-duct was performed by Delot and Garnier [36] from the Onera Group in France. In their work, an array of VG vanes and micro-jet actuators (10-120 ms^{-1}, 14 continuous or pulsed jets) were used on the lower part of an s-duct (Re = 1.5x10^6) showing that VGs (50% or more improvement for 0.15<Ma<0.45 at AIP) are more effective in reducing flow distortion than continuous jets (30% improvement, for Ma 0.2 at AIP) or pulsed jets (50% improvement, for Ma 0.2 at AIP) and yield better results for a wider range of Mach numbers [36].

Table 3 gives a summary of active flow control techniques discussed in this section.

6. Hybrid flow control

A few researchers have combined passive and active flow control techniques in an attempt to control both the steady and time-dependant flow properties in s-shaped intake ducts. This combination of active and passive flow control methods is called a hybrid system.

Table 3: Summary of active flow control techniques employed on s-ducts

flow control	flow regime	separation	distortion	PR	pressure loss	swirl	E/N	publication
wall suction & blowing	Ma=0.7	↑	↑	↑	/	/	E	[59]
automatic adjustable blade	/	/	/	/	↓	↑	E	[60]
synthetic jets	Ma=0.3	↑	/	/	↑	/	E	[61]
3D synthetic jet	Ma=0.43	↑	↑	↑	↑	↑	N	[3]
2D synthetic jets	Ma=0.43	↑	↑	/	/	↑	N	[3]
VG jets	Ma=0.1, Re=7.8x10^5	↑	↑ 25%	↑	↑ 30%	/	E	[62]
tang. blowing (const. area)	Re=4.73x10^4	↑	/	/	↑	↓	E	[37]
VG jets (const. area)	Re=4.73x10^4	↑	/	/	↑	↓	E	[37]
3D control jet	Ma=0.43	↑	↑	↑	/	/	E	[63]
2D control jet	Ma=0.43	↑	↑	- - -	/	/	E	[63]
2D steady blowing	Ma=0.44, Re=7.5x10^5	↑	↑ 13.3%	↑ 1.7%	/	/	E&N	[2]
supersonic pulsed jets	Re=1.5x10^6	↑	↑	↑	/	/	E	[64]
zero-net-mass-flow jet	Re=4.1x10^4	↑	/	/	/	/	E	[66]
Electro-hydrodynamic EHD	Ma=0.3-0.7	↑	↑ 6.7%	↑ 0.34%	/	/	N	[1]
AC-DBD plasma	/	↑	/	/	/	/	E&N	[67]
pulsed micro jet	Re=1.5x10^6	↑	↑ 50%	- - -	/	/	E	[36]
continuous micro jet	Re=1.5x10^6	↑	↑ 30%	- - -	/	/	E	[36]

Symbols indicate: ↑ = improvement by flow control technique; / = not reported; ↓ = deterioration by flow control technique;
- - - = no effect.

Gissen et al. [39, 72] proved that hybrid systems can have an additional benefit on performance parameters, compared to passive or active flow control alone. In [39], the authors employ vane-type VG and synthetic jets at a Mach number of 0.55 in an s-duct with no flow separation in the baseline case. Vane-type VG and synthetic jets both improve the performance parameters when used alone, and decrease the circumferential distortion descriptor by 20% each. The combination of both in the hybrid system has a more profound effect, reducing the distortion by as much as 35%. This is shown in Figure 17. Total pressure contours at the AIP, presented in Figure 16, also demonstrate the combined effect of passive and active flow control. However, as the authors note in their work, caution has to be exercised as some hybrid configurations had a detrimental effect on the performance of the duct.

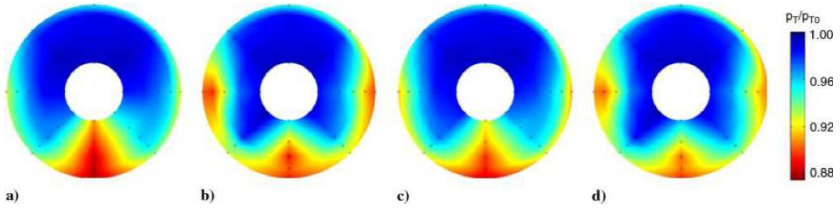

Figure 16: Time averaged total pressure contours at AIP for a) baseline s-duct, b) vane type VG, c) synthetic jets, and d) hybrid flow control. Figure taken from [39].

A second publication [72] explains the dynamics of the hybrid flow control model. As expected, the vane-type VG only have a steady effect, but the synthetic jets, operated at 133 Hz, have a cyclic contribution. Initially, at the begining of the duty cycle, the synthetic jets cause an increase of distortion followed by a stark decrease. Being a viability study, Gissen et al. have not optimised the jet operation for frequency which may result in improving the initial response at the onset of the active flow control.

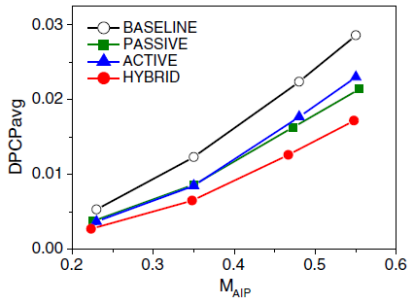

Figure 17: Society of Automotive Engineers circumferential distortion descriptor (DPCP) with Mach number for baseline flow, passive (vane type VG), active (synthetic jets), and hybrid flow control. Figure taken from [39].

Owens et al. also investigated the suitability of hybrid flow control [73]. Their design of vane-type VG and air jets achieved an additional benefit, too. The same decrease of circumferential distortion coefficient at the AIP was recorded for lower air jet mass flows with the hybrid system. This suggests that passive-active hybrid flow control can be a means of making the active part more efficient, by having the passive flow control device improve the steady performance and the active one the time-dependant performance.

Further research is necessary to show that hybrid systems can eliminate flow separation, as existing studies only quantified the improvement in circumferential distortion at the AIP.

7. Conclusions

Passive flow control devices have been heavily studied by a number of researchers and show good results. From the passive flow control devices reviewed, tapered fin vortex generators and submerged vortex generators improved pressure loss and distortion by double digit percentages. It is widely agreed that the optimum location for vortex generators is upstream of the

separation point just ahead of the high adverse pressure gradient. At this location the boundary layer grows rapidly before detaching from the surface and separating. Most early active flow control devices were derived from their passive counterparts (i.e. VG jets) and employed in both continuous and pulsed mode. Three-dimensional synthetic jets and pulsed micro-jets show the greatest promise amongst active flow control devices. While the biggest improvements in flow parameters at first appear to be achieved with optimisation techniques - decreasing distortion values of pressure by as much as 80% - there is doubt over the accuracy of reported benefits because transient features have not been accounted for.

From the survey, it is also evident that passive flow control devices have some detrimental effects such as induced drag. However, active flow control methods do not yet seem mature enough to be employed in real-life scenarios with the risk of no flow control too high should their powering mechanism become dysfunctional. Whereas passive devices are commonplace on aeronautical components, no reports of commercially used active components have been found. It seems, the penalty in added drag of passive devices is worth its price compared to the complexity of active devices which often require separate energy sources or compressed air. Some researchers have tried to address this issue with hybrid flow control methods combining passive and active techniques. This approach shows promise, but is not yet advanced enough to be compared one to one with more mature flow control systems.

Given the recent findings on the unsteadiness of the flow in convoluted ducts and the significant variation to flow parameters as compared to time-

averaged data, it is believed that the effect of flow control techniques should also be obtained with unsteady measurements - both experimentally and numerically.

8. Acknowledgments

The authors are grateful to the Engineering and Physical Sciences Research Council (EPSRC) for their sponsorship of the PhD project. Authors also acknowledge Rolls-Royce's support.

9. References

[1] Y. Hui, L. Feng, S. Yaoying, and S. Baigang, "Numerical investigation of electrohydrodynamic (EHD) flow control in an s-shaped duct," *Plasma Science and Technology*, vol. 14, no. 10, pp. 897–904, 2012.

[2] J. C. Vaccaro, Y. Elimelech, Y. Chen, O. Sahni, K. E. Jansen, and M. Amitay, "Experimental and numerical investigation on steady blowing flow control within a compact inlet duct," *International Journal of Heat and Fluid Flow*, vol. 54, pp. 1143–152, 2015.

[3] Z. J. Chen and J. J. Wang, "Numerical investigation on synthetic jet flow control inside an s-inlet duct," *Science China Technological Sciences*, vol. 55, no. 9, pp. 2584–2578, 2012.

[4] S. R. Wellborn, B. A. Reichert, and T. H. Okiishi, *An experimental investigation of the flow in diffusing s-duct*. PhD thesis, NASA Technical Memorandum 105809, 1992.

[5] B. A. Reichert and B. J. Wendt, "Improving diffusing s-duct performance by secondary flow control," tech. rep., NASA Technical Memorandum 106492, 1994.

[6] S. A. E. Standard, "1419b: Inlet total pressure distortion considerations for gas turbine engines," 2013.

[7] N. C. Bissinger and T. Breuer, *Encyclopedia of Aerospace Engineering, Chapter EAE487; Basic principles Gas turbine compatibility intake aerodynamic aspects*. 2010.

[8] S. A. E. Standard, "1420b: Gas turbine engine inlet flow distortion guidelines," 2011.

[9] R. W. Guo and J. Seddon, "The swirl in an s-duct of typical air intake proportions," *Aeronautical Quarterly*, vol. 34, no. 2, pp. 99–129, 1983.

[10] P. K. Zachos, D. G. MacManus, and N. Chiereghin, "Flow distortion measurements in convoluted aero engine intakes," in *33rd AIAA Applied Aerodynamics Conference*, 2015.

[11] J. C. Vaccaro, Y. Elimelech, Y. Chen, O. Sahni, K. E. Jansen, and M. Amitay, "Experimental and numerical investigation on the flow field within a compact inlet duct," *International Journal of Heat and Fluid Flow*, vol. 44, pp. 478–488, 2013.

[12] A. D. Vakili, J. M. Wu, P. Liver, and M. K. Bhat, "Compressible flow in a diffusing s-duct with flow separation," tech. rep., SEE A87-45831, 1987.

[13] D. Gil-Prieto, D. G. MacManus, P. K. Zachos, G. Tanguy, and K. R. Menzies, "Convoluted intake distortion measurements using stereo particle image velocimetry," in *34th AIAA Applied Aerodynamics Conference*, no. AIAA 2016-3560, 2016.

[14] A. R. Paul, K. Kuppa, M. S. Yadav, and U. Dutta, "Flow improvement in rectangular air intake by submerged vortex generators," *Journal of Applied Fluid Mechanics*, vol. 4, no. 2, pp. 77–86, 2011.

[15] A. Asghar, R. Stowe, W. Allan, and D. Alexander, "Entrance aspect ratio effect on s-duct inlet performance at high-subsonic flow," *Journal of Engineering for Gas Turbines and Power*, vol. 139, May 2017.

[16] G. Tanguy, D. G. MacManus, P. Zachos, and D. Gil-Prieto, "Passive flow control study in an s-duct using stereo particle image velocimetry," *AIAA Journal*, vol. 55, June 2017.

[17] P. Bansod and P. Bradshaw, "The flow in s-shaped ducts," *Aeronautical Quarterly*, vol. 23, no. 2, pp. 131–140, 1972.

[18] A. M. K. P. Taylor, J. H. Whitelaw, and M. Yianneskis, "Developing flows in s-shaped ducts: square cross-section duct," tech. rep., NASA technical report 3550, 1982.

[19] A. M. K. P. Taylor, J. H. Whitelaw, and M. Yianneskis, "Developing flows in s-shaped ducts: circular cross-section duct," tech. rep., NASA technical report 3759, 1984.

[20] A. D. Vakili, J. M. Wu, P. Liver, and M. K. Bhat, "Flow control in a diffusing s-duct," in *AIAA Shear Flow Conference*, 1985.

[21] T. Berens, A. Delot, M. Chevalier, and J. V. Muijden, "Numerical simulations for high offset intake diffuser flows," *AIAA Journal*, 2014.

[22] R. W. Guo and J. Seddon, "An investigation of the swirl in an s-duct," *Aeronautical Quarterly*, vol. 33, no. 1, pp. 25–58, 1982.

[23] Y. T. Ng, S. C. Luo, T. T. Lim, and Q. W. Ho, "On the relation between centrifugal force and radial pressure gradient in flow inside curved s-shaped ducts," *Physics of Fluids*, vol. 20, no. 5 (055109), 2008.

[24] R. K. Sullerey, S. Mishra, and A. M. Pradeep, "Application of BL fences and VG in improving performance of s-duct diffuser," *Transactions of ASME*, vol. 124, pp. 136–142, 2002.

[25] M. J. Brear, Z. Warfield, J. F. Mangus, C. S. Braddom, J. D. Paduano, and J. S. Philhower, "Flow separation within the engine inlet of an uninhabited combat air vehicle," *Transactions of ASME*, vol. 126, pp. 266–272, 2004.

[26] A. S. Luers, "Flow control techniques in a serpentine inlet: an enabling technology to increase the military viability of unmanned air vehicles," Master's thesis, MIT, 2003.

[27] D. G. MacManus, N. Chiereghin, D. Gil-Prieto, and P. Zachos, "Complex aeroenaero intake ducts and dynamic distortion," *AIA Journal*, vol. 55, July 2017.

[28] D. Gil-Prieto, D. G. MacManus, P. K. Zachos, T. G., and K. R. Menzies, "Convoluted intake distortion measurements using stereo particle image velocimetry," *AIAA Journal*, vol. 55, pp. 1878–1892, June 2017.

[29] J. C. Lin, "Review of research on low-profile vortex generators to control boundary-layer separation," *Progress in Aerospace Sciences*, vol. 38, pp. 389–420, 2002.

[30] R. D. M. and K. T. T., "Boundary-layer submerged vortex generators for separation control - an exploratory study," in *AIAA/ASME/SIAM?APS 1st National Fluid Dynamics Congress*, 1988.

[31] J. C. Lin, "Control of turbulent boundary-layer separation using micro-vortex generators," in *30th AIAA Fluid Dynamics Conference*, 1999.

[32] R. W. Guo and J. Seddon, "Swirl characteristics of an s-shaped air intake with both horizontal and vertical offsets," *Aeronautical Quarterly*, vol. 34, no. 2, pp. 130–146, 1983.

[33] B. A. Reichert and B. J. Wendt, "An experimental investigation of s-duct flow control using arrays of low profile vg," tech. rep., NASA Technical Memorandum 106030, 1993.

[34] P. Ashill, J. Fulker, and K. Hackett, "Research at dera on sub boundary layer vortex generators (sbvgs)," in *39th AIAA Aerospace Sciences Meeting and Exhibit*, 2001.

[35] B. J. Wendt, G. I., and H. W.R., "The structure and development of streamwise vortex arrays embedded in a turbulent boundary layer," *AIAA Journal*, no. 92-0551, 1992.

[36] A. L. Delot, E. Garnier, and D. Pagan, "Flow control in a high-offset subsonic air intake," in *47th AIAA/ASME/SAE/ ASEE Joint Propulsion conference*, 2011.

[37] Y. T. Ng, S. C. Luo, T. T. Lim, and Q. W. Ho, "Three techniques to control flow separation in an s-shaped duct," *AIAA*, vol. 49, no. 9, pp. 1825–1832, 2011.

[38] Y. Zhang, S. Hu, X. F. Zhang, M. Benner, A. Mahallati, and E. Vlasic, "Flow control in an aggrssive interturbine transition duct using low profile vortex generators," *Journal of Engineering for Gas Turbines and Power*, vol. 136, no. 11 (112604), 2014.

[39] A. Gissen, B. Vukasinovic, M. McMillan, and A. Glezer, "Distortion management in a boundary layer ingestion inlet diffuser using hybrid flow control," *Journal of Propulsion and Power*, vol. 30, no. 3, pp. 834–844, 2014.

[40] A. R. Paul, P. Ranjan, V. K. Patel, and A. Jain, "Comparative studies on flow control in rectangular s-duct diffuser using submerged vortex generators," *Aerospace Science and Technology*, vol. 28, pp. 332–343, 2013.

[41] L. Jenkins, S. A. Gorton, and A. S., "Flow control device evaluation for an internal flow with an asdverse pressure gradient," in *40th AIAA Aerospace Sciences Meeting and Exhibit*, 2002.

[42] J. B. Parham, M. Fitzgerald, and E. de la Rosa Blanco, "Flow control for boundary layer ingestion in an s-duct diffuser," in *9th AIAA Aerospace Science Meeting*, 2011.

[43] J. W. Hamstra, D. N. Miller, P. P. Truax, B. A. Anderson, and B. J.

Wendt, "Active inlet flow control technology demonstration," *the Aeronautical Journal*, vol. 104, no. 1040, pp. 473–479, 2000.

[44] A. Jirasek, "Design of vortex generators flow control in inlets," *Journal of Aircraft*, vol. 43, no. 6, pp. 1886–1892, 2006.

[45] B. Anderson, D. Miller, G. Addington, and J. Agrell, "Optimal microvane flow control for compact air vehicle inlets," *NASA/TM-2014-212936*, 2004.

[46] J. S. Yi, C. Kim, and B. J. Lee, "Adjoint based design optimisation of vortex generator in an s-shaped subsonic inlet," *AIAA Journal*, vol. 50, no. 11, pp. 2492–2507, 2012.

[47] W. L. Zhang, D. D. Knight, and D. Smith, "Automated design of a three dimensional subsonic diffuser," *Journal of Propulsion and Power*, vol. 16, no. 6, pp. 1132–1139, 2000.

[48] S. Lefantzi and D. D. Knight, "Automated design optimisation of a three dimensional s-shaped subsonic diffuser," *Journal of Propulsion and Power*, vol. 18, no. 4, pp. 913–921, 2002.

[49] A. Aranake, J. G. Lee, D. Knight, R. M. Cummings, J. Cox, M. Paul, and A. R. Byerley, "Automated design optimisation of a three dimensional subsonic diffuser," *Journal of Propulsion and Power*, vol. 27, no. 4, pp. 838–846, 2011.

[50] D. Ghate, A. Isaacs, K. Sudhakar, P. M. Mujumdar, and A. G. Marathe, "3D duct design using variable fidelity method," in *10th AIAA/ISSMO*

Multidisciplinary Analysis and Optimization Conference, no. AIAA 2004-4427, 2004.

[51] A. E. Eiben and J. E. Smith, *Introduction to evolutionary computing - Natural Computing Series*. Springer, 2015.

[52] S. Shahpar, "High fidelity multi-stage design optimisation of multi-stage turbine blades using a mid-range approximate method (MAM)," in *13th AIAA/ISSMO Multidisciplinary Analysis Optimization Conference*, 2010.

[53] S. Shahpar, S. Caloni, and L. de Prieelle, "Automatic design optimisation of profiled endwalls including real geometrical effects to minimise turbine secondary flows," *Journal of Turbomachinery*, vol. 139, no. 7, 2017.

[54] A. Polynkin, V. Toropov, and S. Shahpar, "Multidisciplinary optimisation of turbomachinery based on metamodel built by genetic programming," in *13th AIAA/ISSMO Multidisciplinary Analysis optimisation Conference*, no. AIAA 2010-9397, 2010.

[55] S. Shahpar, "Challenges to overcome for routine usage of automatic optimisation in the propulsion industry," *The Aeronautical Journal*, vol. 115, October 2011.

[56] Y. Korolev, V. Toropov, and S. Shahpar, "Large-scale cfd optimization based on the ffd parametrization using the multipoint approximation method in an hpc environment," *AIAA 2015-3234*, 2015.

[57] Y. Korolev, V. Toropov, and S. Shahpar, "Design optimization under uncertainty using the multipoint approximation method," *AIAA 2017-1934*, 2017.

[58] P. T. Boggs and J. W. Tolle, "Sequential quadratic programming," *Acta Numerica*, vol. 4, pp. 1–51, 1995.

[59] W. H. Ball, "Tests of wall suction and blowing in highly offset diffusers," *Journal of Aircraft*, vol. 22, no. 3, pp. 161–167, 1985.

[60] P. F. Weng and R. W. Guo, "New method of swirl control in a diffusing s-duct," *AIAA Journal*, vol. 30, no. 7, pp. 1918–1919, 1991.

[61] M. Amitay, D. Pitt, and A. Glezer, "Separation control in duct flows," *Journal of Aircraft*, vol. 39, no. 4, pp. 616–620, 2002.

[62] A. M. Pradeep and R. K. Sullerey, "Active flow control in circular and transitioning s-duct diffusers," *Transactions of ASME*, vol. 128, pp. 1192–1203, 2006.

[63] J. C. Vaccaro, Y. Elimelech, and M. Amitay, "Experimental investigation of actuators for flow control in short inlet ducts," in *48th AIAA Aerospace Science Meeting*, 2010.

[64] E. Garnier, M. Leplat, J. C. Monnier, and J. Delva, "Flow control by pulsed jet in highly bended s-duct," in *6th AIAA flow control conference*, 2012.

[65] E. Garnier, "Flow control by pulsed jet in a curved s-duct: a spectral analysis," *AIAA Journal*, vol. 53, no. 10, pp. 2813–2827, 2015.

[66] R. Mathis, D. Duke, V. Kitsios, and J. Soria, "Use of zero-net-mass-flow for separation control in diffusing s-duct," *Experimental Thermal and Fluid Science*, vol. 33, pp. 169–172, 2008.

[67] X. Xu, *Plasma actuation for boundary layer separation control in engine ducts*. PhD thesis, University de Montreal, 2011.

[68] T. Unfer and J. P. Boeuf, "Modelling of a nanosecond surface discharge actuator," *Journal of Physics*, vol. 42, no. 19 (194017), 2009.

[69] G. Correale, "Preliminary investigation on ns-dbd plasma actuator for active flow separation control," Master's thesis, TU Delft, 2011.

[70] D. V. Roupassov, A. A. Nikipelov, M. M. Nudnova, and A. Y. Starikovskii, "Flow separation control by plasma actuator with nanosecond pulsed-periodic discharge," *AIAA Journal*, vol. 47, no. 1, pp. 168–185, 2009.

[71] J. Little, K. Takashima, M. Nishihara, I. Adamovich, and M. Samimy, "Separation control with nanosecond-pulse-driven dielectric barrier discharge plasma actuators," *AIAA Journal*, vol. 50, no. 2, pp. 350–365, 2012.

[72] A. Gissen, B. Vukasinovic, and A. Glezer, "Dynamics of flow control in a nemulated boundary layer ingesting offset diffuser," *Experiments in Fluids*, vol. 55, no. 1794, 2014.

[73] L. Owens, B. Allan, and S. Gorton, "Boundary-layer-ingesting inlet flow control," *Journal of Aircraft*, vol. 45, pp. 1431–1440, July-August 2008.